PNAS

Supplementary Information for

Structures of Human Gastrin-Releasing Peptide Receptors Bound to Antagonist and Agonist for Cancer and Itch Therapy.

Shuman Peng[1], Yuting Zhan[1], Dongqi Zhang[1], Lu Ren[1], Anqi Chen[1], Xiaokun Shen[2], Zhoufeng Chen[3], Haitao Zhang [1, 4, *].

[1]Hangzhou Institute of Innovative Medicine, Institute of Pharmacology and Toxicology, Zhejiang Province Key Laboratory of Anti-Cancer Drug Research, College of Pharmaceutical Sciences, Zhejiang University, Hangzhou, Zhejiang, China;

[2]Convalife (Shanghai) Co., Ltd., Shanghai, China;

[3]Center for the Study of Itch and Sensory Disorders, Departments of Anesthesiology, Medicine, Psychiatry, and Developmental Biology, Washington University School of Medicine, St Louis, MO, USA;

[4]The Second Affiliated Hospital, Zhejiang University School of Medicine, Hangzhou, Zhejiang, China.

Haitao Zhang

Email: haitaozhang@zju.edu.cn

This PDF file includes:

Figures S1 to S6

Tables S1 to S5

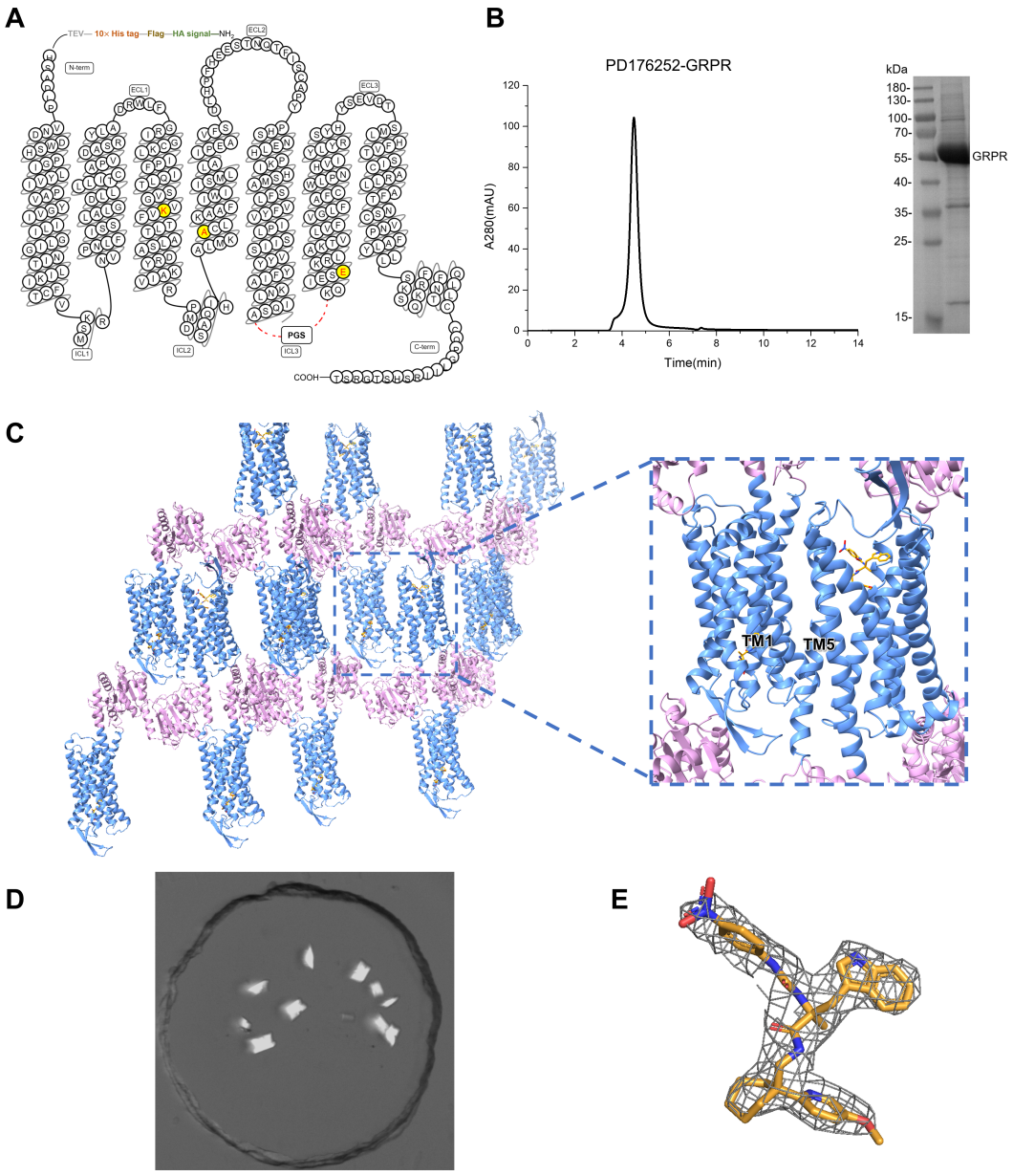

Figure S1. Generation of GRPR constructs for crystallography.

(A) Snake plot of the GRPR crystallized construct.

(B) Size exclusion chromatography profile and SDS-PAGE analysis of the purified GRPR-PD176252 proteins.

(C) Crystal packing of GRPR-PD176252. GRPR, PD176252, and PGS were shown as blue ribbons, orange sticks, and plum ribbons, respectively.

(D) Image of GRPR-PD176252 crystals grown in lipidic cubic phase.

(E) |2Fo|-|Fc| map (gray mesh) contoured at 1.0 σ of the non-peptide antagonist PD176252 (orange).

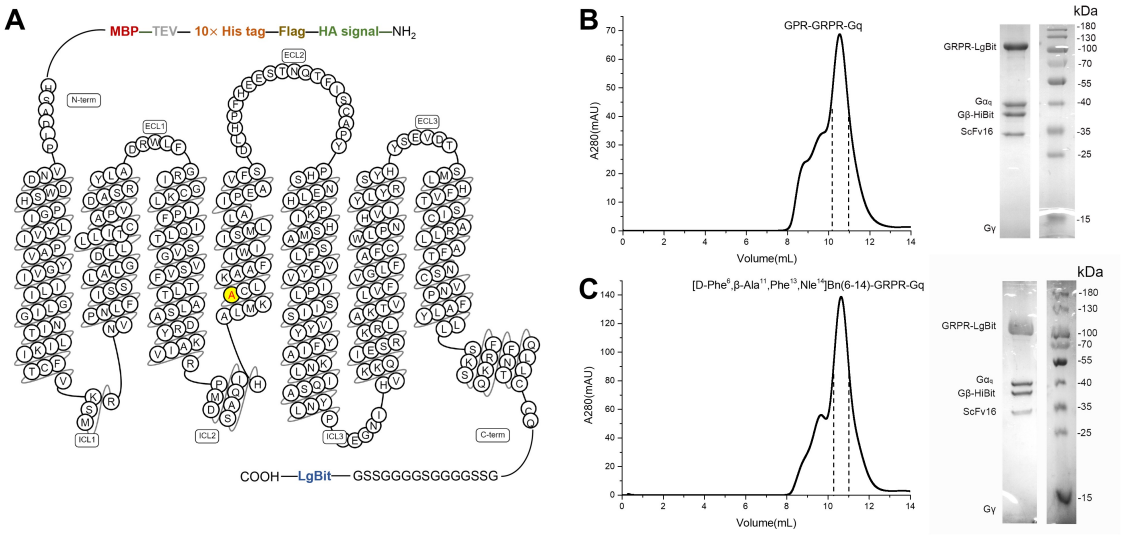

Figure S2. Construct design and purification of the GRPR-G_q proteins with agonists.

(A) Snake plot of the GRPR cryo-EM construct.

(B, C) Size-exclusion chromatography elution profile and SDS-PAGE analysis of the purified GRPR-G_q proteins in complex with GRP (B) and [D-Phe^6, β-Ala^{11}, Phe^{13}, Nle^{14}] Bn (6-14) (C).

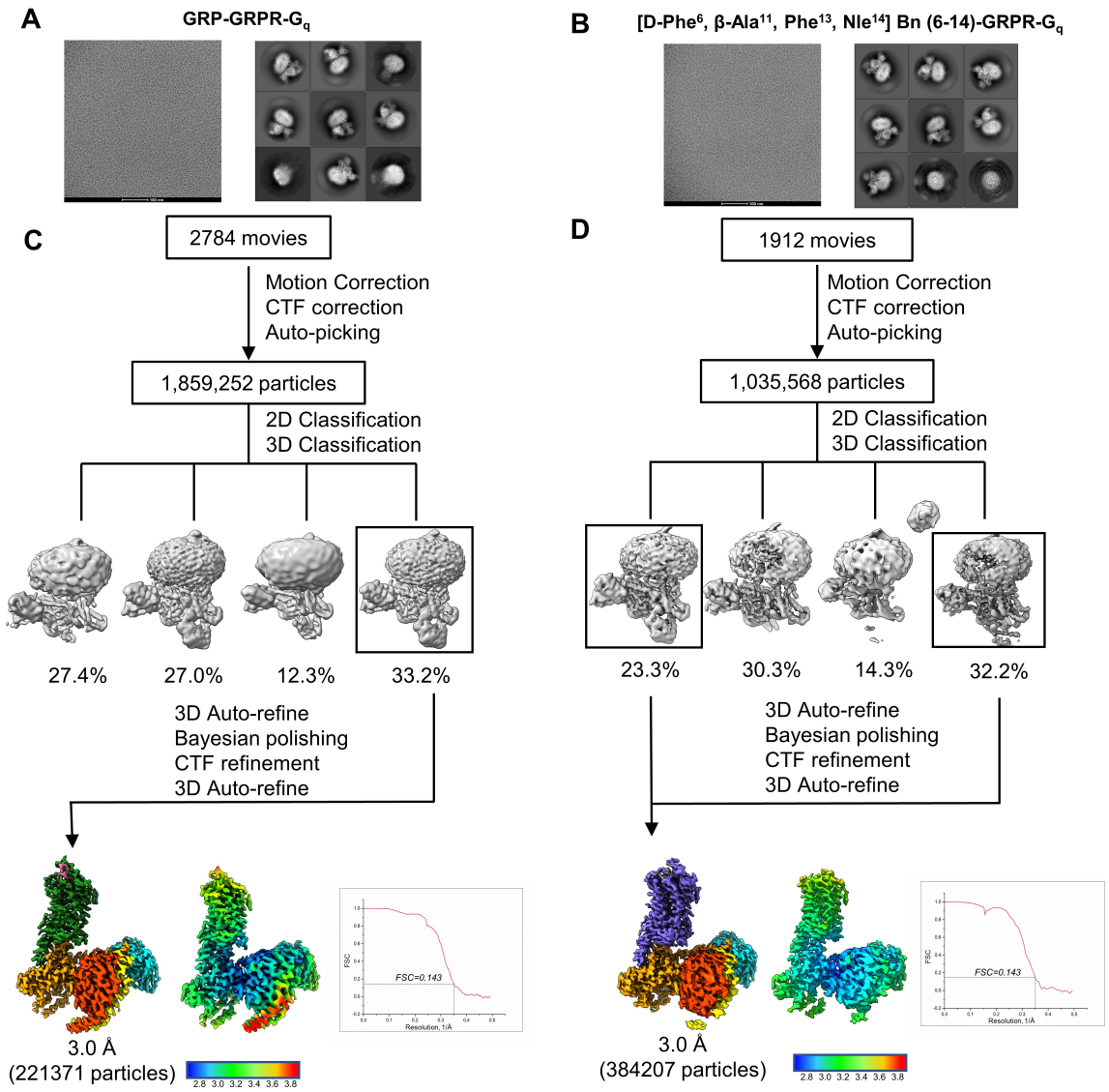

Figure S3. Cryo-EM images and data-processing of GRPR-G_q complex.

(A) Representative cryo-EM micrograph (scale bar, 100 nm) of GRP-GRPR-G_q complex particles imaged at a nominal 73k × magnification and representative two-dimensional class averages.

(B) Representative cryo-EM micrograph (scale bar, 100 nm) of [D-Phe^6, β-Ala^{11}, Phe^{13}, Nle^{14}] Bn (6-14)-GRPR-G_q complex particles imaged at a nominal 73k× magnification and representative two-dimensional class averages.

(C) Flow chart of the cryo-EM data processing for the GRP-GRPR-G_q complex.

(D) Flow chart of the cryo-EM data processing for the [D-Phe^6, β-Ala^{11}, Phe^{13}, Nle^{14}] Bn (6-14)-GRPR-G_q complex.

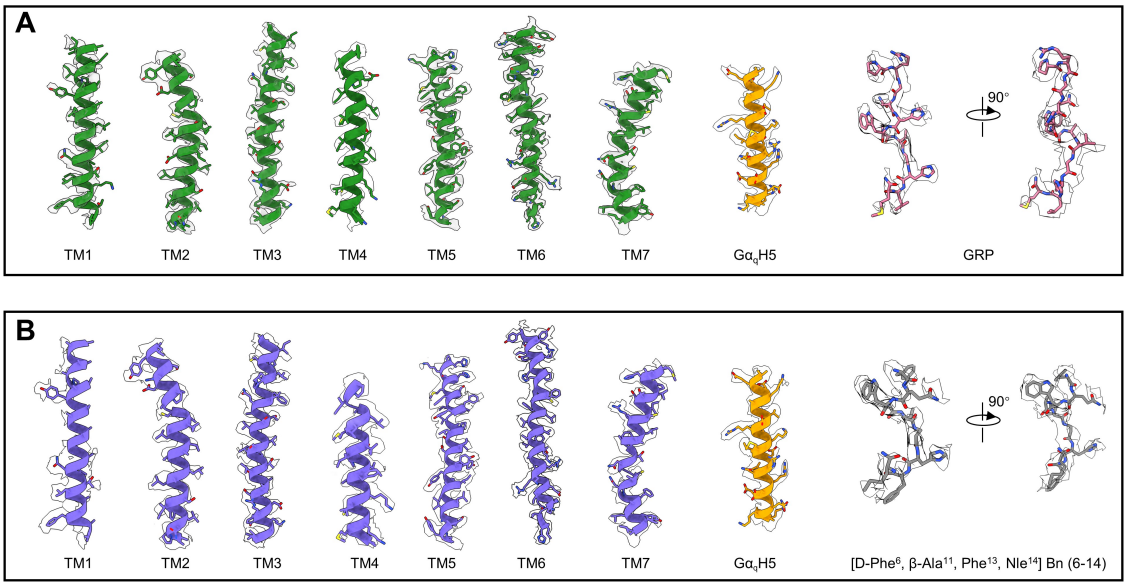

Figure S4. The cryo-EM density maps for GRPR-G_q complexes.

(A) Cryo-EM density maps of TMs1-7, GRP, and α5 helix of $G\alpha_q$ in the GRP-GRPR-G_q structure.

(B) Cryo-EM density maps of TMs1-7, [D-Phe^6, β-Ala^{11}, Phe^{13}, Nle^{14}] Bn (6-14), and α5 helix of $G\alpha_q$ in the [D-Phe^6, β-Ala^{11}, Phe^{13}, Nle^{14}] Bn (6-14)-GRPR-G_q structure.

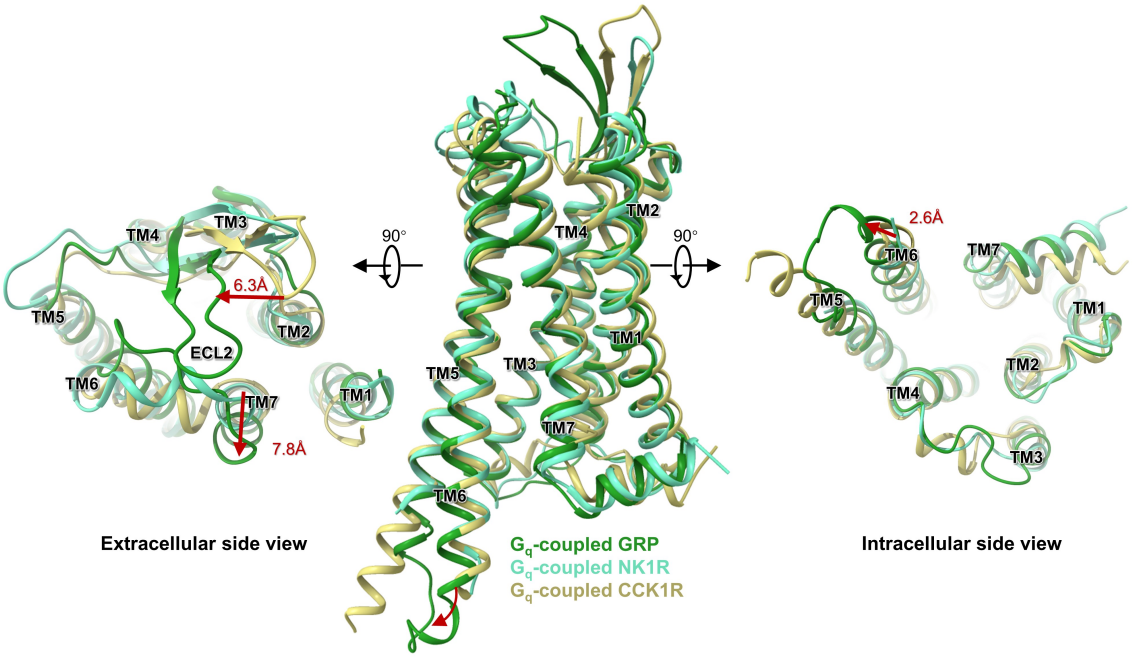

Figure S5. Structural comparison of GRPR with G_q-coupled NK_1R and CCK_1R. Different views of the structural superposition of GRPR (forest green), NK_1R (medium aquamarine, PDB ID: 7RMG), and CCK_1R (dark khaki, PDB ID: 7EZM).

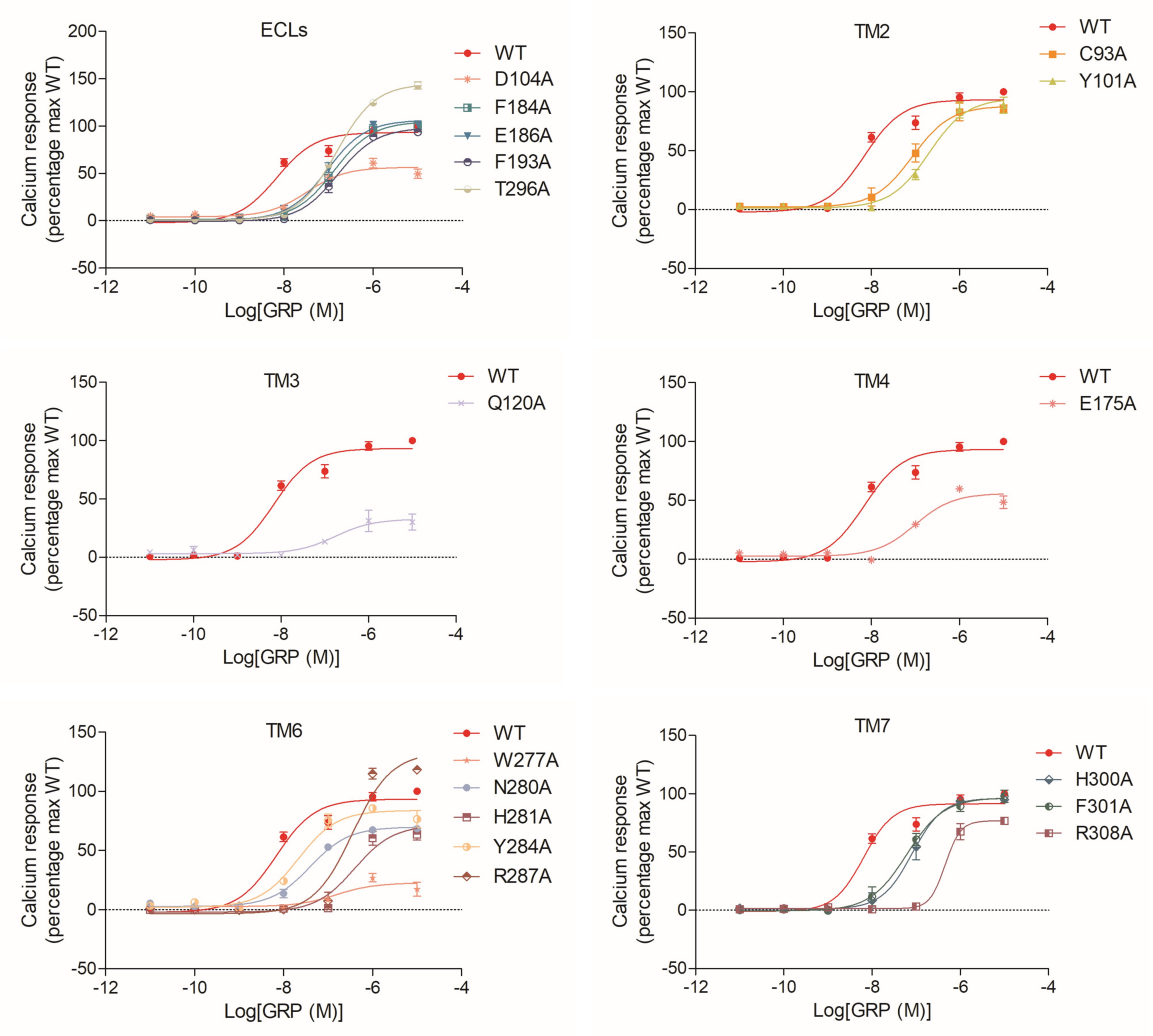

Figure S6. Effects of mutations in the ligand-binding pocket of GRPR on the GRP-induced calcium mobilization. Data represented the Mean ± S.E.M., n=3 independent replicates. WT represented wild type. Source data are provided as a Source Data file.

Table S1. Crystallographic data collection and refinement statistics

	GRPR-PD176252
PDB ID	7W41
Data collection	
Space group	*C* 1 2 1
Cell dimensions	
a, b, c (Å)	134.104, 60.025, 98.489
α, β, γ (°)	90.00, 113.57, 90.00
Resolution (Å)	50.00-2.95 (3.06-2.95)
R_{merge}	0.151 (0.599)
$I/\sigma I$	8.14 (1.11)
*CC**	0.994 (0.908)
Completeness (%)	96.9 (95.8)
Redundancy	4.0 (3.5)
Refinement	
Resolution (Å)	27.75-2.95 (3.06-2.95)
No. reflections	14,788 (1,449)
R_{work} / R_{free}	0.281/0.286
No. atoms	3,909
Average *B*-factors (Å^2)	88.4
R.m.s.deviations	
Bond lengths (Å)	0.01
Bond angles (°)	1.56
Ramachandran plot (%)	
Favored	98.35
Allowed	1.65
Disallowed	0

#Data from 4 crystal were used to solve the structure.

*Highest resolution shell was shown in parenthesis.

Table S2. Effects of mutagenesis in the ligand-binding pocket of GRPR on the GRP-induced calcium mobilization. E_{max} and pEC_{50} values were presented as Mean ± S.E.M. from three independent experiments. Source data are provided as a Source Data file.

Mutations	**Locations**	E_{max}	pEC_{50}
WT		93.38±4.24	8.16±0.10
C93A	2.57	88.01±2.54	7.07±0.06
Y101A	2.65	94.52±3.11	6.70±0.07
D104A	ECL1	56.51±3.35	7.48±0.15
Q120A	3.32	32.70±3.17	6.76±0.23
E175A	4.60	55.59±4.28	7.01±0.17
F184A	ECL2	104.8±2.38	6.87±0.05
E186A	ECL2	98.11±2.68	6.80±0.06
F193A	ECL2	106.4±2.32	7.04±0.05
W277A	6.48	22.57±3.35	6.82±0.35
N280A	6.51	69.84±1.87	7.40±0.07
H281A	6.52	83.91±3.84	7.67±0.11
Y284A	6.55	71.42±4.76	6.40±0.13
R287A	6.58	132.6±7.90	6.45±0.12
T296A	ECL3	143.7±3.01	6.83±0.08
H300A	7.31	96.16±3.08	7.09±0.21
F301A	7.32	96.61±3.00	7.21±0.12
R308A	7.39	76.79±1.78	6.34±0.48

Table S3. Effects of the GRPR-G_q cryo-EM constructs on the GRP-induced calcium mobilization. E_{max} and pEC50 values were presented as Mean ± S.E.M. from three independent experiments. Source data are provided as a Source Data file.

GRPR	**G_q**	***E_{max}***	**pEC_{50}**
WT	WT	93.38±4.24	8.16±0.10
Cryo-EM	WT	97.68±3.75	7.78±0.09
WT	Cryo-EM	79.49±2.68	6.60±0.07
Cryo-EM	Cryo-EM	89.69±4.83	6.38±0.11

Table S4. Effects of the E186^{ECL2}A in GRPR on the [D-Phe^{6}, β-Ala^{11}, Phe^{13}, Nle^{14}] Bn (6-14) induced calcium mobilization. Data are presented as the Mean ± S.E.M. (n = 3) of three independent experiments performed in triplicate.

Mutantions	**Locations**	E_{max}	pEC_{50}
WT		90.28±4.42	7.82±0.16
E186A	ECL2	95.69±3.74	8.02±0.12

Table S5. Cryo-EM data collection and refinement statistics of the GRP-GRPR and GRPR-[D-Phe^{6}, βAla^{11}, Phe^{13}, Nle^{14}] Bn (6-14) complex structures

	GRPR-G_q-GRP	**GRPR-G_q- [D-Phe^{6}, βAla^{11}, Phe^{13}, Nle^{14}] Bn (6-14)**
PDB ID/EMDB ID	7W3Z/EMD-32297	7W40/EMD-32298
Data collection and processing		
Magnification	29000×	29000×
Voltage (kV)	300	300
Electron exposure (e-/Å^2)	64	64
Defocus range (μm)	-1.1~-1.3	-1.10~-1.25
Pixel size (Å)	1.014	0.507
Symmetry imposed	C1	C1
Initial particle projections (no.)	1,859,252	1,380,329
Final particle projections (no.)	577,387	222,542
Map resolution (Å)	3.0	3.0
FSC threshold	0.143	0.143
Map resolution range (Å)	2.5-4.5	2.5-4.5
Refinement		
Initial model used	7F6G	7F6G
Model resolution (Å)	3.1	3.2
FSC threshold	0.5	0.5
Map sharpening *B* factor (Å^2)	83.24929	80.24929
Model composition		
Non-hydrogen atoms	10,221	9,236
Protein residues	1,295	1,176
B factors (Å^2)	46.99	42.65
R.m.s.deviations		
Bond lengths (Å)	0.010	0.010
Bond angles (°)	1.359	1.383
Validation		
MolProbity score	1.56	1.74
Clashscore	5.90	7.11
Rotamer outliers (%)	1.52	1.93
Ramachandran plot		
Favored (%)	97.50	97.41
Allowed (%)	2.50	2.59

Disallowed (%)	0	0

88